

<sup>1</sup> **Mediterranean drought variability over the last millennium**

Benjamin I Cook<sup>1,2</sup>, Kevin J Anchukaitis<sup>3</sup>, Ramzi Touchan<sup>4</sup>, David M Meko<sup>4</sup>,

and Edward R Cook<sup>5</sup>

---

Corresponding author: Benjamin I Cook, NASA Goddard Institute for Space Studies, New York, New York, USA. (benjamin.i.cook@nasa.gov)

<sup>1</sup>NASA Goddard Institute for Space Studies, New York, New York, USA.

<sup>2</sup>Ocean and Climate Physics,  
Lamont-Doherty Earth Observatory,  
Palisades, New York, USA.

<sup>3</sup>Woods Hole Oceanographic Institution,  
Woods Hole, Massachusetts, USA.

<sup>4</sup>Laboratory of Tree-Ring Research,  
University of Arizona, Tucson, Arizona,  
USA.

<sup>5</sup>Tree Ring Laboratory, Lamont-Doherty  
Earth Observatory, Palisades, New York,  
USA.

**Abstract.** Recent droughts in the Mediterranean have highlighted concerns that anthropogenic climate change may be contributing to recent drying trends, but the full range of natural climate variability in the region is still poorly understood. Here, we analyze 900 years (1100–2012) of Mediterranean drought variability in the Old World Drought Atlas (OWDA), a spatiotemporal tree-ring based reconstruction of the June–July–August self calibrating Palmer Drought Severity Index. In the Mediterranean, the OWDA is highly correlated with spring precipitation (April–June), the North Atlantic Oscillation (January–April), the Scandinavian Pattern (January–March), and the East Atlantic Pattern (April–June). Drought variability in the basin shows significant east-west coherence on multi-decadal to centennial time scales, contrary to previous analyses. We also find significant North-South antiphasing in the eastern Mediterranean, with a tendency for the Black Sea region (e.g., Greece, Anatolia, the Balkans, etc) to be wet when coastal Libya, the southern Levant, and the Mideast are dry, possibly related to variability in the North Atlantic Oscillation. Recent droughts are centered in the western Mediterranean, Greece, and the Levant region. Events of similar magnitude in the western Mediterranean and Greece are apparent in the OWDA back to 1100 CE, but the most recent 15-year drought in the Levant (1998–2012) appears as the driest such period in the record. Estimating sampling uncertainties using a Monte-Carlo approach, we conclude that there is an 89% likelihood that the recent Levant drought is drier than any comparable period

<sup>25</sup> of the last 900 years, possibly indicating the emergence of a greenhouse gas  
<sup>26</sup> forced drying signal.

## 1. Introduction

27 Climate change impacts on water resources are a significant concern in the regions sur-  
28 rounding the Mediterranean Sea [*Iglesias et al.*, 2007; *García-Ruiz et al.*, 2011], an area  
29 including southern Europe, Northern Africa, and the Levant (Cyprus, Israel, Jordan,  
30 Lebanon, Palestine, Syria, Turkey) region of the Middle East. Projections from climate  
31 models almost uniformly point towards drying in the Mediterranean from increased green-  
32 house gas forcing in the coming decades [*Giorgi and Lionello*, 2008; *Seager et al.*, 2014],  
33 part of an overall trend towards desiccation and poleward expansion of subtropical dry  
34 zones [*Held and Soden*, 2006; *Seager et al.*, 2010]. Indeed, analyses of recent climate trends  
35 in the region suggest that this process may have already begun [*García-Ruiz et al.*, 2011;  
36 *Gleick*, 2014; *Hoerling et al.*, 2012; *Kelley et al.*, 2012, 2015].

37 However, a more complete understanding of natural Mediterranean drought variability  
38 and anthropogenic moisture trends requires comparisons with longer term variability than  
39 is observable from relatively short instrumental records. To this end, the paleoclimate  
40 community has been active throughout this region, developing estimates of Common Era  
41 drought variability from a variety of proxies, including tree-rings [*Choukri et al.*, 1995;  
42 *Glueck and Stockton*, 2001; *Touchan et al.*, 2003; *Akkemik and Aras*, 2005; *Touchan et al.*,  
43 2005; *Esper et al.*, 2007; *Andreu et al.*, 2007; *Nicault et al.*, 2008; *Touchan et al.*, 2008a;  
44 *Büntgen et al.*, 2010; *Touchan et al.*, 2011; *Köse et al.*, 2011; *Touchan et al.*, 2014a],  
45 sediment cores [e.g., *Jones et al.*, 2006; *Roberts et al.*, 2012; *Moreno et al.*, 2012], and  
46 speleothems [e.g., *Jex et al.*, 2011; *Wassenburg et al.*, 2013]. To date, however, there is  
47 little consensus across these different records regarding the character and dominant drivers

48 of drought variability across the basin over the last millennium. In particular, there are  
49 extant uncertainties regarding how widespread droughts are in the Mediterranean [Roberts  
50 *et al.*, 2012], the magnitude and timing of long-term trends and centennial-scale variability  
51 [Esper *et al.*, 2007; Touchan *et al.*, 2011; Wassenburg *et al.*, 2013], and how seasonal  
52 signals and large-scale climate modes are reflected in proxy reconstructions [Touchan  
53 *et al.*, 2014a, b; Seim *et al.*, 2014].

54 Given these uncertainties, the development and analyses of new large-scale reconstruc-  
55 tions is imperative for improving our understanding of regional climate dynamics in the  
56 Mediterranean region. Here, we use a spatially resolved tree-ring based field reconstruction  
57 of European and Mediterranean drought to investigate the dominant spatial and temporal  
58 patterns of drought variability across the basin over the last millennium. Specifically, our  
59 analysis addresses three primary research questions: 1) What are the dominant modes  
60 of hydroclimate variability in the Mediterranean? 2) How spatially coherent are drought  
61 events across the Mediterranean basin? and 3) How do recent droughts compare to long-  
62 term hydroclimate variability over the last millennium?

## 2. Materials and Methods

### 2.1. The Old World Drought Atlas

63 The Old World Drought Atlas [OWDA; Cook *et al.*, in revision] is a new, tree-ring based re-  
64 construction of summer season (June-July-August, JJA) self calibrating Palmer Drought  
65 Severity Index (scPDSI) [van der Schrier *et al.*, 2013]. The OWDA uses 106 tree-ring  
66 chronologies to reconstruct scPDSI at 5,414 half degree grid points for the entire Common  
67 Era over the European-Mediterranean domain ( $27^{\circ}\text{N}$ – $71^{\circ}\text{N}$ ,  $12^{\circ}\text{W}$ – $45^{\circ}\text{E}$ ). The reconstruc-  
68 tion uses the point-by-point method [Cook *et al.*, 1999, 2013] with a search radius of 1000

69 kilometers, meaning any grid cell can be reconstructed from proxy predictor series within  
70 1000 kilometers. Proxy site locations in the Mediterranean portion of the OWDA ( $30^{\circ}\text{N}$ –  
71  $47^{\circ}\text{N}$ ,  $10^{\circ}\text{W}$ – $45^{\circ}\text{E}$ ) are shown in Figure 1, along with the approximate start date of the  
72 various records. We restrict our analysis to 1100–2012 CE, the interval during which the  
73 Mediterranean domain is reasonably well covered by proxy sites. Values in the OWDA  
74 up through 1978 are tree-ring reconstructed; from 1979–2012 the OWDA incorporates the  
75 instrumental scPDSI.

76 The scPDSI is a modification of the original PDSI formulation of *Palmer* [1965], a  
77 locally normalized drought index incorporating changes in supply (precipitation), demand  
78 (evapotranspiration) and storage (soil moisture). PDSI has an inherent memory timescale  
79 of 12–18 months [*Guttmann*, 1998; *Vicente-Serrano et al.*, 2010], allowing the JJA target of  
80 the OWDA to incorporate climate information from the previous winter and spring, the  
81 main seasons of moisture supply to the Mediterranean. The scPDSI used as the target for  
82 the OWDA reconstruction is calculated from version TS3.21 of the high-resolution CRU  
83 climate grids [*Harris et al.*, 2014], incorporates a snow module, and uses the Penman–  
84 Monteith formulation for calculating potential evapotranspiration [*van der Schrier et al.*,  
85 2013].

## 2.2. Climate Data

86 Monthly precipitation data used in the analyses are from the high-resolution CRU gridded  
87 climate data [TS3.21, *Harris et al.*, 2014]. We also use monthly average indices from the  
88 Climate Prediction Center from climate modes previously shown to have an influence on  
89 Mediterranean climate [*Sousa et al.*, 2011]. The North Atlantic Oscillation [NAO; *Hurrell*,  
90 1995] consists of a north-south dipole in atmospheric pressure between Greenland and the

91 subtropical North Atlantic, with positive phases typically associated with below-average  
92 precipitation in the Mediterranean and southern Europe. The Scandinavian Pattern [SCA;  
93 *Bueh and Nakamura, 2007*] is centered over Scandinavia, with positive height anomalies in  
94 this region causing above-average precipitation across central and southern Europe. The  
95 East Atlantic Pattern [EA; *Barnston and Livezey, 1987*] is similar to the NAO, consisting  
96 of a north-south anomaly dipole in the Atlantic. Unlike the NAO, however, the EA has  
97 stronger connections to the subtropical ridge. Positive phases of the EA are linked to  
98 below average precipitation across southern Europe. For the CRU precipitation data and  
99 the climate indices, we restrict our analysis for the most recent period when data quality  
100 and availability is highest (1950–2012).

### 2.3. Analyses

101 We use Spearman's rank correlations to assess the statistical relationship between recon-  
102 structions, observations, and indices. Spearman's is a non-parametric alternative to the  
103 Pearson product-moment correlation that is less sensitive to outliers. We also conduct  
104 spectral and spectral coherency analyses using a multi-taper approach [*Thomson, 1982*;  
105 *Chave et al., 1987; Mann and Lees, 1996; Czaja and Marshall, 2001; Huybers, 2004*] with  
106 significance levels estimated using a non-parametric Monte Carlo procedure with red noise  
107 (AR1) conditioned on the original data. We also use wavelet coherency analyses [*Maraun  
and Kurths, 2004; Maraun et al., 2007*] to investigate time-varying coherency between var-  
108 ious drought series. In some figures, smoothing of time series by a 10-year lowess linear fit  
109 was applied to emphasize low frequency variability, although all statistical analyses were  
110 conducted on the original (unfiltered) data.

### 3. Results

#### 3.1. Climate Signals in the OWDA

Correlations between winter (January–March; JFM) and spring (April–June) precipitation and the tree-ring reconstructed JJA scPDSI are uniformly positive across the basin (Figure 2). The strongest correlations with JFM precipitation are localized in Spain and Morocco in the western Mediterranean and the Levant region in the eastern basin. MAM precipitation correlations are more uniform and strongly positive across nearly the entire Mediterranean, suggesting that the summer season soil moisture variability, reflected in the OWDA and the underlying tree growth, is driven primarily by spring precipitation [c.f. *Touchan et al.*, 2014a].

Climate mode correlations with the CRU precipitation data or the OWDA scPDSI (Figure 3) are consistent in sign, but generally stronger in the precipitation data. The weaker OWDA scPDSI correlations are expected for at least two reasons. First, these climate modes reflect shifts in atmospheric circulation that have a direct impact on precipitation by modulating, for example, storm track positions and moisture convergence. Circulation impacts on the scPDSI will be by definition more indirect, as the scPDSI is computed based on departures of a variety of variables from climatologically expected values (e.g., soil moisture). Additionally, up to year 1978, the scPDSI is reconstructed as a scaled linear function of the underlying tree-ring proxies, which contains additional uncertainties in the estimates of scPDSI.

The influence of the NAO is strongest in winter and early spring (January–April; JFMA). Positive phases of the NAO cause drying across the northern reaches of the Mediterranean basin, from Spain and Morocco across to the Balkans and western Turkey,

133 while favoring wetter conditions in coastal regions of Libya, Egypt, and the Levant. Con-  
134 sistent with both the instrumental observations [e.g. *Lamb et al.*, 1997; *Knippertz et al.*,  
135 2003] and the underlying controls on tree growth [*Touchan et al.*, 2008a, b; *Panayotov  
et al.*, 2010], the influence of the NAO in the OWDA is strongest in the far western part  
137 of the domain and the Balkans. The largest influence of the SCA pattern is during the  
138 winter (JFM), with positive phases increasing moisture across most of the basin. The SCA  
139 correlation with the OWDA is substantially weaker, consistent with previously analyses  
140 (Figure 2) demonstrating the much stronger connection between the OWDA and spring  
141 season, rather than winter, precipitation. Unlike the previous two modes, the influence of  
142 the EA is highest during the spring (AMJ), causing widespread drying across the basin  
143 with, notably, similar magnitude correlations with both precipitation and scPDSI.

### 3.2. Drought Variability in the OWDA

144 Figure 4 shows OWDA scPDSI averaged over the Mediterranean domain and the fractional  
145 land area in drought ( $\text{scPDSI} \leq -1$ ) for each year from 1100–2012. Inter-annual variability  
146 (standard deviation) in the scPDSI is 0.54 standardized PDSI units and, on average, 29%  
147 of the basin experiences drought conditions in any given year. Highlighted are several  
148 example periods of persistent multi-year droughts and pluvials (Figure 4, grey bars).  
149 Noticeably absent are any extended multi-decadal (30-year or longer) ‘megadroughts’, a  
150 characteristic feature of North American drought variability during the Medieval Climate  
151 Anomaly (approximately before 1300 CE) [e.g., *Cook et al.*, 2010] and previously inferred  
152 from Moroccan tree-rings [*Esper et al.*, 2007].

153 The spatial expression of the six highlighted periods of widespread drought (and one  
154 pluvial) are shown in Figure 5. The most dramatic wet interval was a nearly two-decade

long period from 1125–1142 CE, with sustained wet conditions in modern day Spain,  
155 Morocco, Algeria, Tunisia, Italy, the Balkans, and Turkey. Among the five highlighted  
156 persistent drought events, there is a tendency for simultaneous drought in the extreme  
157 western (Spain, Morocco, Algeria, Tunisia) and eastern (Balkans, Greece, Turkey) ends  
158 of the basin. This is somewhat contrary to previous analyses of other proxy records in the  
159 region, which have suggested instead a tendency for an antiphased dipole in hydroclimate  
160 variability between these two regions [e.g., *Roberts et al.*, 2012]. The basin-wide synchrony  
161 found in these example events is further confirmed by compositing all years when at least  
162 40% or 50% of the basin is in drought (Figure 6). Here, again, we can see the major poles  
163 of synchronous and severe drought during these years of widespread drought are centered  
164 over the opposite ends of the basin. In these events and composite, however, there is  
165 some evidence for antiphasing in the eastern end of the basin, where there is a tendency  
166 for Libya, Egypt and the southern Levant to be wet or near normal when Greece and  
167 Anatolia are in drought. This meridional dipole structure bears some resemblance to the  
168 NAO correlation patterns with precipitation and scPDSI (Figure 3).

### 3.3. Spatial Synchrony

To further investigate the tendency for synchronous hydroclimate variability across the  
170 basin, we averaged scPDSI from the OWDA over three regions: the western Mediterranean  
171 (WestMED; 32°N–42°N, 10°W–0°E), the eastern Mediterranean (EastMED; 36°N–41°N,  
172 20°E–37°E), and an area encompassing coastal Egypt, the southern Levant, and other ar-  
173 eas of the Middle East (MidEast; 30°N–34°N, 33°E–47°E). The first two areas (WestMED  
174 and EastMED) chosen correspond to approximately the same areas used in the analysis  
175 of *Roberts et al.* [2012]. Point-by-point correlations (Figure 7) between these three indices

and the OWDA are strongly positive at the local level, as expected, decaying in magnitude outside of the averaging regions. For WestMED the correlations remain mostly positive, or near zero, across the entire basin. EastMED, however, shows strong negative correlations over Libya, Egypt, and the Levant while MidEast is negatively correlated with a large region surrounding the Black Sea. As with the drought composites (previous section), these results again suggest a strong tendency for meridional antiphasing in hydroclimate in the eastern Mediterranean Basin, with a pattern similar to what would be expected due to precipitation responses to variations in the NAO.

Spectral analyses of WestMED and EastMED show significant power in both series at high (inter-annual) and low (decadal to multidecadal) frequencies (Figure 8). Both have significant peaks at about 3–4 years, with EastMED additionally peaking at decadal frequencies and WestMED covering a broader range of multi-decadal bands. The two regions also overlap in their power at around 70 years, though EastMED is only marginally significant at the 90<sup>th</sup> percentile. A coherency spectra analysis between the two regional indices demonstrates highly significant coherence between the two regions over inter-annual and decadal timescales (Figure 9). Notably, there is also a broad band of coherence between the two region at multi-decadal and centennial timescales (30 to 130 years), despite no significant spectral peaks at wavelengths longer than ~75 years in either WestMED or EastMED. This may be due to aliasing of shared frequencies: both series have peaks at around 70-75 years, approximately the first harmonic of the 130 year coherence reflected in the coherency spectra. An analysis of the relative phasing for these spectral bands (not shown) indicates that the null hypothesis (i.e., ‘WestMED and EastMED are in phase’) can NOT be rejected at the  $p \leq 0.05$  significance level. These results are further confirmed

200 by a cross-wavelet coherency analysis (Figure 10). These results show that EastMED and  
201 WestMED share significant variance in the decadal to centennial frequency bands for most  
202 of the analysis period and that these two series are primarily in phase (i.e., black arrows  
203 point to the right). Further, EastMED and MidEast have significant coherence at inter-  
204 annual to multidecadal frequencies, but are largely 180 degrees out of phase (i.e., blacks  
205 arrows are primarily pointing to 90 degrees to the left). These results indicate that, at  
206 least over the last millennium, there is a reasonably strong tendency for in-phase drought  
207 in the zonal direction across the Mediterranean, in sharp contrast to the inferences made  
208 by *Roberts et al.* [2012].

### 3.4. Recent Droughts

209 Recent decades have witnessed persistent, multi-year droughts in the Mediterranean that  
210 have spurred speculation that warming induced drying trends may have begun to emerge.  
211 In the OWDA, these droughts are not coherent across the Mediterranean basin but are  
212 instead highly localized in the WestMED region, Greece ( $36^{\circ}\text{N}$ – $43^{\circ}\text{N}$ ,  $19^{\circ}\text{E}$ – $26^{\circ}$ ), and the  
213 Levant ( $30^{\circ}\text{N}$ – $37^{\circ}\text{N}$ ,  $33^{\circ}\text{E}$ – $40^{\circ}\text{E}$ ) (Figure 11). Both WestMED and Greece experienced  
214 significant droughts in the 1980s and 1990s that have since ameliorated. The driest period  
215 in the Levant began in 1998 and has been generally ongoing since. Here, we attempt to  
216 place these most recent drought events within the context of OWDA drought variability  
217 for the last 900 years (Figure 12).

218 Over the last 30 years (1980–2012), we identify major periods of persistent drought in  
219 all three of these regions: 1980–2009 (WestMED), 1984–2002 (Greece), and 1998–2012  
220 (Levant) (Figure 13, black dots). For each region, we then calculate the driest previous  
221 interval of the same length (Figure 13, grey dots). For both of these intervals, we estimate

222 sampling uncertainties (the whiskers) using a Monte-Carlo procedure where we resample  
223 drought years from each interval with replacement, recalculating the mean scPDSI 10,000  
224 times. The whiskers represent the 25<sup>th</sup> and 75<sup>th</sup> percentiles of these resampled means.

225 In general agreement with *Touchan et al.* [2008a], the recent persistent droughts in  
226 WestMED and Greece qualify as the most severe on the record. In both regions, how-  
227 ever, there is substantial overlap in the uncertainties, and the recent droughts are not  
228 significantly drier (Student's t-test and Wilcoxon rank sum test,  $p > 0.10$ ) than the pre-  
229 vious driest intervals. From this, we conclude that, while severe, recent droughts in the  
230 WestMED region and Greece are not statistically separable from natural drought vari-  
231 ability over the last 900 years.

232 The magnitude of the recent Levant drought exceeds the magnitude of the driest  
233 previous interval in the region. In the Levant, mean scPDSI for 1998–2012 is  $-1.52$ ,  
234 compared to  $-1.1$  for 1205–1219, with non-overlapping confidence limits between the  
235 two events. Despite this separation, 1998–2012 is not significantly drier than the pre-  
236 vious driest period (One-Sided Student's t-test,  $p = 0.13$ ). This is likely due to the  
237 leveraging of the mean scPDSI for 1998–2012 by several extremely dry years: 1999  
238 (scPDSI=  $-3.25$ ), 2000 (scPDSI=  $-4.49$ , the driest single year in this region back to  
239 1100), 2008 (scPDSI=  $-2.80$ ), and 2012 (scPDSI=  $-2.72$ ). In 89% of our Monte-Carlo  
240 simulations, however, the resampled mean scPDSI for 1998–2012 was drier than the re-  
241 sampled mean for the previous driest interval, 1205–1219. We therefore conclude that it  
242 is likely that 1998–2012 in the Levant was the driest 15-year period of the last 900 years,  
243 suggesting the possible emergence of a greenhouse gas forced drying signal.

#### 4. Discussion and Conclusions

Paleoclimate reconstructions provide better sampling of the full spectrum of natural variability in the climate system, variability that is often not adequately captured by the relatively short instrumental record. This knowledge is especially critical for identifying decadal and multidecadal variability and for evaluating the extent to which anthropogenic forcing may be influencing recent climate trends and events. But while a variety of local reconstruction efforts have been previously undertaken for the Mediterranean, field reconstructions provide an opportunity to understand natural and anthropogenic patterns at broader spatial and extended temporal scales.

Our analysis of the OWDA shows significant decadal to multi-decadal variability in hydroclimate across the Mediterranean, with significant coherence between the western and eastern basin centers on multi-decadal to centennial time scales and meridional antiphasing in the eastern Mediterranean Basin. The dynamics driving these patterns are still uncertain, but the NAO or processes linked to the North Atlantic are likely to be a major contributor [*Hurrell and Loon, 1997; Eshel and Farrell, 2000*]. The NAO mode is negatively correlated with precipitation and scPDSI across most of the basin (Figure 2) and at the decadal scale is associated with same-sign wet season (boreal winter) precipitation anomalies from Morocco and the Iberian Peninsula though western and central Anatolia, with opposing anomalies in the Levant [*Mariotti et al., 2002; Xoplaki et al., 2004*]. And while there is a zonal dipole in the Mediterranean tree-ring response to precipitation, with a stronger winter response to the west and an increasing spring-summer signal in the east [*Touchan et al., 2014a, b*], at decadal timescales at least the summer scPDSI does appear to reflect the broad-scale forcing of precipitation anomalies associated

266 with the NAO. This creates a basin-wide coherence between northwestern Africa, the  
267 Balkans, and western Anatolia (Figure 9) and opposite sign anomalies in the Levant  
268 during major Mediterranean drought and pluvial events (Figure 5–7).

269 Interestingly, this coherent decadal pattern is somewhat different than that observed  
270 for recent scPDSI trends (Figure 11–13), with the western Mediterranean and the Levant  
271 experiencing more substantial drying trends, and with mixed signs over Anatolia. This  
272 suggests that NAO variability alone may not account for recent drought trends, and  
273 supports interpretations that greenhouse gas forcing has an important influence [Kelley  
274 *et al.*, 2012, 2015; Seager *et al.*, 2014]. Although some climate model simulations suggest  
275 recent NAO trends are outside the range of natural variability [Osborn, 2004; Kuzmina  
276 *et al.*, 2005], long control simulations can demonstrate unforced NAO variability similar  
277 to that seen in recent decades [Semenov *et al.*, 2008]. Drying in the Levant is also likely  
278 influenced by recent trends toward a more positive EA pattern [Krichak *et al.*, 2002;  
279 Krichak and Alpert, 2005; Lim, 2014].

280 Our findings here suggest that, at least in the western Mediterranean and Greece,  
281 the recent severe decadal-scale dry conditions are not yet outside the range of natural  
282 variability, despite the influence of greenhouse gas forcing. In the Levant, however, we  
283 estimate that the last 15 years are likely the driest since the 12<sup>th</sup> century. Drought  
284 conditions here reduce water supply in the face of increasing demand, and create the  
285 potential for sociopolitical and economic disruption [e.g. Gleick, 2014; Kelley *et al.*, 2015],  
286 requiring a multidisciplinary research, management, and policy approach [Sohl and van  
287 Ginkel, 2014]. To that end, paleoclimate field reconstructions of drought can provide

288 valuable information on the long-term and broad-scale context of recent events, especially  
289 how they fit within the context of natural climate variability.

290 **Acknowledgments.** Funding for Anchukaitis, Meko, and Touchan provided by NSF  
291 Earth System History Grant #ESH0317288. Lamont contribution #.

## References

- 292 Akkemik, U., and A. Aras (2005), Reconstruction (1689-1994 AD) of April-August pre-  
293 cipitation in the southern part of central Turkey, *International Journal of Climatology*,  
294 25(4), 537–548, doi:10.1002/joc.1145.
- 295 Andreu, L., E. Gutiérrez, M. Macias, M. Ribas, O. Bosch, and J. J. Camarero (2007),  
296 Climate increases regional tree-growth variability in Iberian pine forests, *Global Change  
297 Biology*, 13(4), 804–815, doi:DOI:10.1111/j.1365-2486.2007.01322.x.
- 298 Barnston, A. G., and R. E. Livezey (1987), Classification, Seasonality and Persistence  
299 of Low-Frequency Atmospheric Circulation Patterns, *Monthly Weather Review*, 115(6),  
300 1083–1126, doi:10.1175/1520-0493(1987)115<1083:CSAPOL>2.0.CO;2.
- 301 Bueh, C., and H. Nakamura (2007), Scandinavian pattern and its climatic impact,  
302 *Quarterly Journal of the Royal Meteorological Society*, 133(629), 2117–2131, doi:  
303 DOI:10.1002/qj.173.
- 304 Büntgen, U., D. Frank, V. Trouet, and J. Esper (2010), Diverse climate sensitivity  
305 of Mediterranean tree-ring width and density, *Trees*, 24(2), 261–273, doi:10.1007/  
306 s00468-009-0396-y.
- 307 Chave, A. D., D. J. Thomson, and M. E. Ander (1987), On the robust estimation of  
308 power spectra, coherences, and transfer functions, *Journal of Geophysical Research:*

- 309      *Atmospheres*, 92(B1), 633, doi:10.1029/jb092ib01p00633.
- 310      Chbouki, N., C. W. Stockton, and D. Myers (1995), Spatio-temporal patterns of drought  
311      in Morocco, *International Journal of Climatology*, 15, 187–205, doi:DOI:10.1002/joc.  
312      3370150205.
- 313      Cook, E. R., D. M. Meko, D. W. Stahle, and M. K. Cleaveland (1999), Drought re-  
314      constructions for the continental United States, *Journal of Climate*, 12(4), 1145–1162,  
315      doi:[http://dx.doi.org/10.1175/1520-0442\(1999\)012<1145:DRFTCU>2.0.CO;2](http://dx.doi.org/10.1175/1520-0442(1999)012<1145:DRFTCU>2.0.CO;2).
- 316      Cook, E. R., R. Seager, R. R. Heim Jr, R. S. Vose, C. Herweijer, and C. Woodhouse  
317      (2010), Megadroughts in North America: placing IPCC projections of hydroclimatic  
318      change in a long-term palaeoclimate context, *Journal of Quaternary Science*, 25(1),  
319      48–61, doi:10.1002/jqs.1303.
- 320      Cook, E. R., P. J. Krusic, K. J. Anchukaitis, B. M. Buckley, T. Nakatsuka, and  
321      M. Sano (2013), Tree-ring reconstructed summer temperature anomalies for tem-  
322      perate East Asia since 800 C.E., *Climate Dynamics*, 41(11-12), 2957–2972, doi:  
323      10.1007/s00382-012-1611-x.
- 324      Cook, E. R., R. Seager, Y. Kushnir, K. R. Briffa, U. Büntgen, D. Frank, P. J. Krusic,  
325      et al. (in revision), Old World Droughts and Pluvials During the Common Era, *Science  
326      Advances*.
- 327      Czaja, A., and J. Marshall (2001), Observations of atmosphere-ocean coupling in the  
328      north atlantic, *Q.J Royal Met. Soc.*, 127(576), 1893–1916, doi:10.1002/qj.49712757603.
- 329      Eshel, G., and B. F. Farrell (2000), Mechanisms of eastern Mediterranean rainfall vari-  
330      ability, *Journal of the Atmospheric Sciences*, 57(19), 3219–3232.

- 331 Esper, J., D. Frank, U. Büntgen, A. Verstege, J. Luterbacher, and E. Xoplaki (2007), Long-  
332 term drought severity variations in Morocco, *Geophysical Research Letters*, 34(17),  
333 L17702, doi:10.1029/2007GL030844.
- 334 García-Ruiz, J. M., J. I. López-Moreno, S. M. Vicente-Serrano, T. Lasanta-Martínez, and  
335 S. Beguería (2011), Mediterranean water resources in a global change scenario, *Earth-*  
336 *Science Reviews*, 105(3–4), 121 – 139, doi:<http://dx.doi.org/10.1016/j.earscirev.2011.01.006>.
- 337 Giorgi, F., and P. Lionello (2008), Climate change projections for the Mediterranean  
338 region, *Global and Planetary Change*, 63(2–3), 90 – 104, doi:<http://dx.doi.org/10.1016/j.gloplacha.2007.09.005>, mediterranean climate: trends, variability and change.
- 341 Gleick, P. H. (2014), Water, Drought, Climate Change, and Conflict in Syria, *Weather,*  
342 *Climate, and Society*, 6(3), 331–340, doi:10.1175/WCAS-D-13-00059.1.
- 343 Glueck, M. F., and C. W. Stockton (2001), Reconstruction of the North Atlantic Os-  
344 cillation, 1429–1983, *International Journal of Climatology*, 21, 1453–1465, doi:DOI:  
345 10.1002/joc.684.
- 346 Guttman, N. B. (1998), Comparing the Palmer Drought Index and the Standardized  
347 Precipitation Index, *Journal of the American Water Resources Association*, 34, 113–  
348 121, doi:10.1111/j.1752-1688.1998.tb05964.x.
- 349 Harris, I., P. D. Jones, T. J. Osborn, and D. H. Lister (2014), Updated high-resolution  
350 grids of monthly climatic observations –the CRU TS3.10 Dataset, *International Journal*  
351 *of Climatology*, 34(3), 623–642, doi:10.1002/joc.3711.
- 352 Held, I. M., and B. J. Soden (2006), Robust Responses of the Hydrological Cycle to  
353 Global Warming, *Journal of Climate*, 19(21), 5686–5699, doi:<http://dx.doi.org/10.1175/JCLI3875.1>.

- 354 1175/JCLI3990.1.
- 355 Hoerling, M., J. Eischeid, J. Perlwitz, X. Quan, T. Zhang, and P. Pegion (2012), On the  
356 Increased Frequency of Mediterranean Drought, *Journal of Climate*, 25(6), 2146–2161,  
357 doi:10.1175/JCLI-D-11-00296.1.
- 358 Hurrell, J. W. (1995), Decadal Trends in the North Atlantic Oscillation: Regional Tem-  
359 peratures and Precipitation, *Science*, 269(5224), 676–679, doi:10.1126/science.269.5224.  
360 676.
- 361 Hurrell, J. W., and H. V. Loon (1997), Decadal Variations in Climate Associated with  
362 the North Atlantic Oscillation, in *Climatic Change at High Elevation Sites*, pp. 69–94,  
363 Springer Netherlands, doi:10.1007/978-94-015-8905-5\_4.
- 364 Huybers, P. (2004), Comments on ‘coupling of the hemispheres in observations and sim-  
365 ulations of glacial climate change’ by a. schmittner, o.a. saenko, and a.j. weaver’, *Qua-*  
366 *ternary Science Reviews*, 23(1-2), 207–210, doi:10.1016/j.quascirev.2003.08.001.
- 367 Iglesias, A., L. Garrote, F. Flores, and M. Moneo (2007), Challenges to Manage the  
368 Risk of Water Scarcity and Climate Change in the Mediterranean, *Water Resources*  
369 *Management*, 21(5), 775–788, doi:10.1007/s11269-006-9111-6.
- 370 Jex, C. N., A. Baker, J. M. Eden, W. J. Eastwood, I. J. Fairchild, M. J. Leng, L. Thomas,  
371 and H. J. Sloane (2011), A 500 yr speleothem-derived reconstruction of late autumn–  
372 winter precipitation, northeast Turkey, *Quaternary Research*, 75(3), 399–405, doi:  
373 DOI:10.1016/j.yqres.2011.01.005.
- 374 Jones, M. D., C. N. Roberts, M. J. Leng, and M. Türkes (2006), A high-resolution late  
375 Holocene lake isotope record from Turkey and links to North Atlantic and monsoon  
376 climate, *Geology*, 34(5), 361–364, doi:doi:10.1130/G22407.1.

- <sup>377</sup> Kelley, C., M. Ting, R. Seager, and Y. Kushnir (2012), The relative contributions  
<sup>378</sup> of radiative forcing and internal climate variability to the late 20th Century win-  
<sup>379</sup> ter drying of the Mediterranean region, *Climate Dynamics*, 38(9-10), 2001–2015, doi:  
<sup>380</sup> 10.1007/s00382-011-1221-z.
- <sup>381</sup> Kelley, C. P., S. Mohtadi, M. A. Cane, R. Seager, and Y. Kushnir (2015), Climate change  
<sup>382</sup> in the Fertile Crescent and implications of the recent Syrian drought, *Proceedings of the*  
<sup>383</sup> *National Academy of Sciences*, 112(11), 3241–3246, doi:10.1073/pnas.1421533112.
- <sup>384</sup> Knippertz, P., M. Christoph, and P. Speth (2003), Long-term precipitation variability  
<sup>385</sup> in Morocco and the link to the large-scale circulation in recent and future climates,  
<sup>386</sup> *Meteorology and Atmospheric Physics*, 83(1), 67–88, doi:10.1007/s00703-002-0561-y.
- <sup>387</sup> Köse, N., U. Akkemik, H. N. Dalfes, and M. S. Özeren (2011), Tree-ring reconstructions  
<sup>388</sup> of May–June precipitation for western Anatolia, *Quaternary Research*, 75(3), 438–450,  
<sup>389</sup> doi:10.1016/j.yqres.2010.12.005.
- <sup>390</sup> Krichak, S., P. Kishcha, and P. Alpert (2002), Decadal trends of main Eurasian oscilla-  
<sup>391</sup> tions and the Eastern Mediterranean precipitation, *Theoretical and Applied Climatology*,  
<sup>392</sup> 72(3-4), 209–220.
- <sup>393</sup> Krichak, S. O., and P. Alpert (2005), Decadal trends in the east Atlantic–west Russia  
<sup>394</sup> pattern and Mediterranean precipitation, *International Journal of Climatology*, 25(2),  
<sup>395</sup> 183–192, doi:10.1002/joc.1124.
- <sup>396</sup> Kuzmina, S. I., L. Bengtsson, O. M. Johannessen, H. Drange, L. P. Bobylev, and M. W.  
<sup>397</sup> Miles (2005), The North Atlantic Oscillation and greenhouse-gas forcing, *Geophysical*  
<sup>398</sup> *Research Letters*, 32(4), doi:10.1029/2004gl021064.

- 399 Lamb, P. J., , M. E. Hamly, and D. H. Portis (1997), North Atlantic Oscillation, *Geo*  
400 *Observateur*, 7, 103–113.
- 401 Lim, Y.-K. (2014), The East Atlantic/West Russia (EA/WR) teleconnection in the North  
402 Atlantic: climate impact and relation to Rossby wave propagation, *Climate Dynamics*,  
403 doi:10.1007/s00382-014-2381-4.
- 404 Mann, M. E., and J. M. Lees (1996), Robust estimation of background noise and signal de-  
405 tection in climatic time series, *Clim. Change*, 33(3), 409–445, doi:10.1007/BF00142586.
- 406 Maraun, D., and J. Kurths (2004), Cross wavelet analysis: significance testing and pitfalls,  
407 *Nonlinear Processes in Geophysics*, 11(4), 505–514, doi:10.5194/npg-11-505-2004.
- 408 Maraun, D., J. Kurths, and M. Holschneider (2007), Nonstationary Gaussian processes  
409 in wavelet domain: Synthesis, estimation, and significance testing, *Phys. Rev. E*, 75,  
410 016,707, doi:10.1103/PhysRevE.75.016707.
- 411 Mariotti, A., M. V. Struglia, N. Zeng, and K. Lau (2002), The hydrological cycle in the  
412 Mediterranean region and implications for the water budget of the Mediterranean Sea,  
413 *Journal of climate*, 15(13), 1674–1690, doi:[http://dx.doi.org/10.1175/1520-0442\(2002\)015<1674:THCITM>2.0.CO;2](http://dx.doi.org/10.1175/1520-0442(2002)015<1674:THCITM>2.0.CO;2).
- 414
- 415 Moreno, A., A. Pérez, J. Frigola, V. Nieto-Moreno, M. Rodrigo-Gámiz, B. Martrat,  
416 P. González-Sampériz, M. Morellón, C. Martín-Puertas, J. P. Corella, et al. (2012),  
417 The Medieval Climate Anomaly in the Iberian Peninsula reconstructed from marine  
418 and lake records, *Quaternary Science Reviews*, 43, 16–32, doi:DOI:10.1016/j.quascirev.  
419 2012.04.007.
- 420 Nicault, A., S. Alleaume, S. Brewer, M. Carrer, P. Nola, and J. Guiot (2008), Mediter-  
421 ranean drought fluctuation during the last 500 years based on tree-ring data, *Climate*

- 422      *Dynamics*, 31(2-3), 227–245, doi:10.1007/s00382-007-0349-3.
- 423      Osborn, T. (2004), Simulating the winter North Atlantic Oscillation: the roles of inter-  
424      national variability and greenhouse gas forcing, *Climate Dynamics*, 22(6-7), doi:10.1007/  
425      s00382-004-0405-1.
- 426      Palmer, W. C. (1965), Meteorological drought, *Tech. rep.*, US Weather Bureau, Wash-  
427      ington, DC.
- 428      Panayotov, M., P. Bebi, V. Trouet, and S. Yurukov (2010), Climate signal in tree-ring  
429      chronologies of *Pinus peuce* and *Pinus heldreichii* from the Pirin Mountains in Bulgaria,  
430      *Trees*, 24(3), 479–490, doi:10.1007/s00468-010-0416-y.
- 431      Roberts, N., A. Moreno, B. L. Valero-Garcés, J. P. Corella, M. Jones, S. Allcock, J. Wood-  
432      bridge, M. Morellón, J. Luterbacher, E. Xoplaki, et al. (2012), Palaeolimnological evi-  
433      dence for an east–west climate see-saw in the Mediterranean since AD 900, *Global and*  
434      *Planetary Change*, 84, 23–34, doi:DOI:10.1016/j.gloplacha.2011.11.002.
- 435      Seager, R., N. Naik, and G. A. Vecchi (2010), Thermodynamic and Dynamic Mechanisms  
436      for Large-Scale Changes in the Hydrological Cycle in Response to Global Warming,  
437      *Journal of Climate*, 23(17), 4651–4668, doi:10.1175/2010JCLI3655.1.
- 438      Seager, R., H. Liu, N. Henderson, I. Simpson, C. Kelley, T. Shaw, Y. Kushnir, and  
439      M. Ting (2014), Causes of Increasing Aridification of the Mediterranean Region in  
440      Response to Rising Greenhouse Gases, *Journal of Climate*, 27(12), 4655–4676, doi:  
441      10.1175/JCLI-D-13-00446.1.
- 442      Seim, A., K. Treydte, V. Trouet, D. Frank, P. Fonti, W. Tegel, M. Panayotov,  
443      L. Fernández-Donado, P. Krusic, and U. Büntgen (2014), Climate sensitivity of Mediter-  
444      ranean pine growth reveals distinct east–west dipole, *International Journal of Clima-*

- <sup>445</sup> *tology, Early View*, doi:10.1002/joc.4137.
- <sup>446</sup> Semenov, V. A., M. Latif, J. H. Jungclaus, and W. Park (2008), Is the observed NAO vari-  
<sup>447</sup> ability during the instrumental record unusual?, *Geophysical Research Letters*, 35(11),  
<sup>448</sup> doi:10.1029/2008gl033273.
- <sup>449</sup> Sohl, M., and M. van Ginkel (2014), Drought preparedness and drought mitigation in the  
<sup>450</sup> developing worlds drylands, *Weather and Climate Extremes*, 3, 62 – 66, doi:[http://dx.  
doi.org/10.1016/j.wace.2014.03.003](http://dx.doi.org/10.1016/j.wace.2014.03.003), high Level Meeting on National Drought Policy.
- <sup>451</sup> Sousa, P. M., R. M. Trigo, P. Aizpurua, R. Nieto, L. Gimeno, R. Garcia-Herrera, P. Li-  
<sup>452</sup> onello, and M. Maugeri (2011), Trends and extremes of drought indices throughout the  
<sup>453</sup> 20th century in the Mediterranean, *Natural Hazards & Earth System Sciences*, 11(1),  
<sup>454</sup> 33 – 51, doi:doi:10.5194/nhess-11-33-2011.
- <sup>455</sup> Thomson, D. J. (1982), Spectrum estimation and harmonic analysis, *Proceedings of the  
IEEE*, 70, 1055–1096.
- <sup>456</sup> Touchan, R., G. M. Garfin, D. M. Meko, G. Funkhouser, N. Erkan, M. K. Hughes, and  
<sup>457</sup> B. S. Wallin (2003), Preliminary reconstructions of spring precipitation in southwestern  
<sup>458</sup> Turkey from tree-ring width, *International Journal of Climatology*, 23(2), 157–171, doi:  
<sup>459</sup> DOI:10.1002/joc.850.
- <sup>460</sup> Touchan, R., E. Xoplaki, G. Funkhouser, J. Luterbacher, M. K. Hughes, N. Erkan,  
<sup>461</sup> U. Akkemik, and J. Stephan (2005), Reconstructions of spring/summer precipitation for  
<sup>462</sup> the Eastern Mediterranean from tree-ring widths and its connection to large-scale atmo-  
<sup>463</sup> spheric circulation, *Climate Dynamics*, 25(1), 75–98, doi:10.1007/s00382-005-0016-5.
- <sup>464</sup> Touchan, R., K. J. Anchukaitis, D. M. Meko, S. Attalah, C. Baisan, and A. Aloui (2008a),  
<sup>465</sup> Long term context for recent drought in northwestern Africa, *Geophysical Research  
Letters*, 35(11), 62–66, doi:10.1029/2008gl033273.

- 468      Letters, 35(13), L13,705, doi:DOI:10.1029/2008GL034264.
- 469      Touchan, R., D. Meko, and A. Aloui (2008b), Precipitation reconstruction for North-  
470      western Tunisia from tree rings, *Journal of Arid Environments*, 72(10), 1887–1896,  
471      doi:10.1016/j.jaridenv.2008.05.010.
- 472      Touchan, R., K. J. Anchukaitis, D. M. Meko, M. Sabir, S. Attalah, and A. Aloui (2011),  
473      Spatiotemporal drought variability in northwestern Africa over the last nine centuries,  
474      *Climate Dynamics*, 37(1–2), 237–252, doi:10.1007/s00382-010-0804-4.
- 475      Touchan, R., K. J. Anchukaitis, V. V. Shishov, F. Sivrikaya, J. Attieh, M. Ketmen,  
476      J. Stephan, I. Mitsopoulos, A. Christou, and D. M. Meko (2014a), Spatial Patterns of  
477      eastern Mediterranean climate influence on tree growth, *The Holocene*, 24(4), 381–392,  
478      doi:10.1177/0959683613518594.
- 479      Touchan, R., D. M. Meko, and K. J. Anchukaitis (2014b), Dendroclimatology in the  
480      Eastern Mediterranean, *Tree-Ring Research*, *in press*.
- 481      van der Schrier, G., J. Barichivich, K. R. Briffa, and P. D. Jones (2013), A scPDSI-based  
482      global data set of dry and wet spells for 1901–2009, *Journal of Geophysical Research:*  
483      *Atmospheres*, doi:10.1002/jgrd.50355.
- 484      Vicente-Serrano, S. M., S. Beguería, J. I. López-Moreno, M. Angulo, and A. El Kenawy  
485      (2010), A new global 0.5 gridded dataset (1901-2006) of a multiscalar drought index:  
486      comparison with current drought index datasets based on the Palmer Drought Severity  
487      Index, *Journal of Hydrometeorology*, 11(4), 1033–1043, doi:<http://dx.doi.org/10.1175/2010JHM1224.1>.
- 488      Wassenburg, J. A., A. Immenhauser, D. K. Richter, A. Niedermayr, S. Riehelmann,  
489      J. Fietzke, D. Scholz, K. P. Jochum, J. Fohlmeister, A. Schröder-Ritzrau, et al. (2013),

- 491 Moroccan speleothem and tree ring records suggest a variable positive state of the North  
492 Atlantic Oscillation during the Medieval Warm Period, *Earth and Planetary Science*  
493 *Letters*, 375, 291–302, doi:DOI:10.1016/j.epsl.2013.05.048.
- 494 Xoplaki, E., J. González-Rouco, J. Luterbacher, and H. Wanner (2004), Wet season  
495 Mediterranean precipitation variability: influence of large-scale dynamics and trends,  
496 *Climate Dynamics*, 23(1), doi:10.1007/s00382-004-0422-0.

## Tree–Ring Chronologies

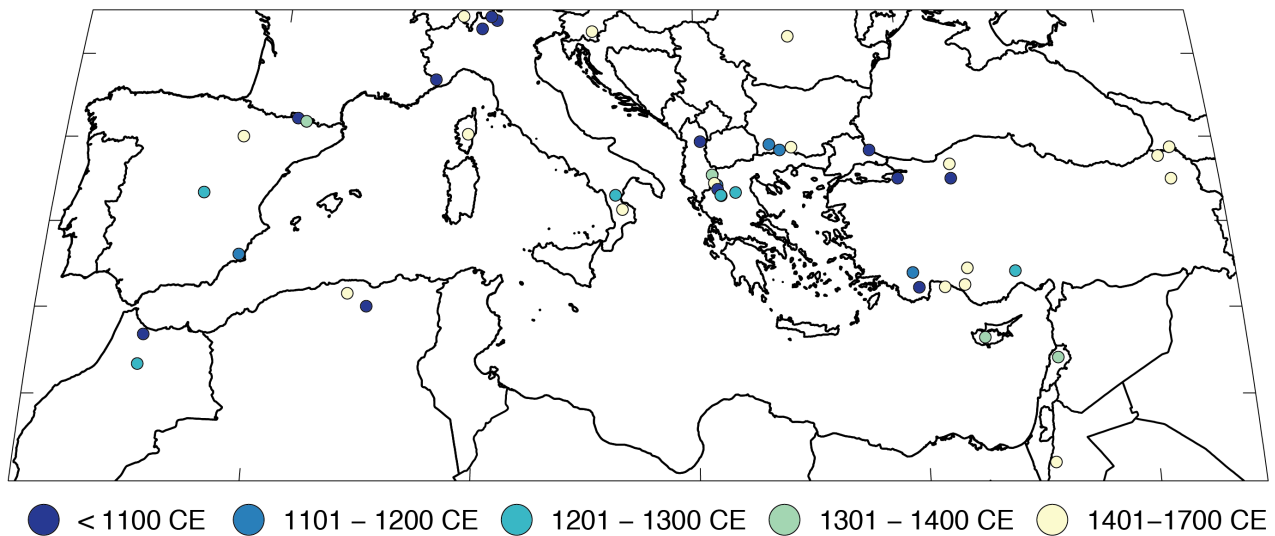


**Figure 1.** Locations of tree-ring chronologies used for the Mediterranean portion of the Old World Drought Atlas. Colors indicate the start dates of the various chronologies.

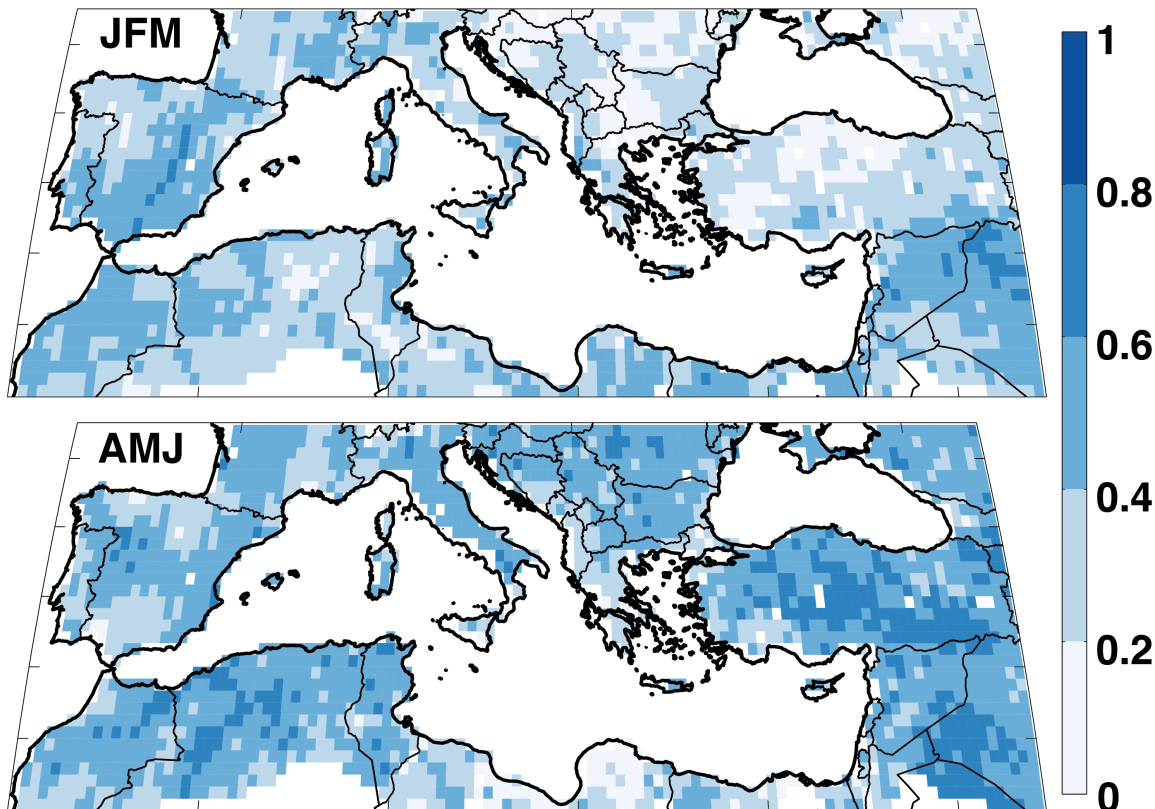


**Figure 2.** Point-by-point Spearman's rank correlation coefficients between CRU 3.21 pre-  
cipitation totals (JFM and AMJ) and OWDA summer season (JJA) scPDSI. Correlations are  
calculated over the period 1950–2012 CE.

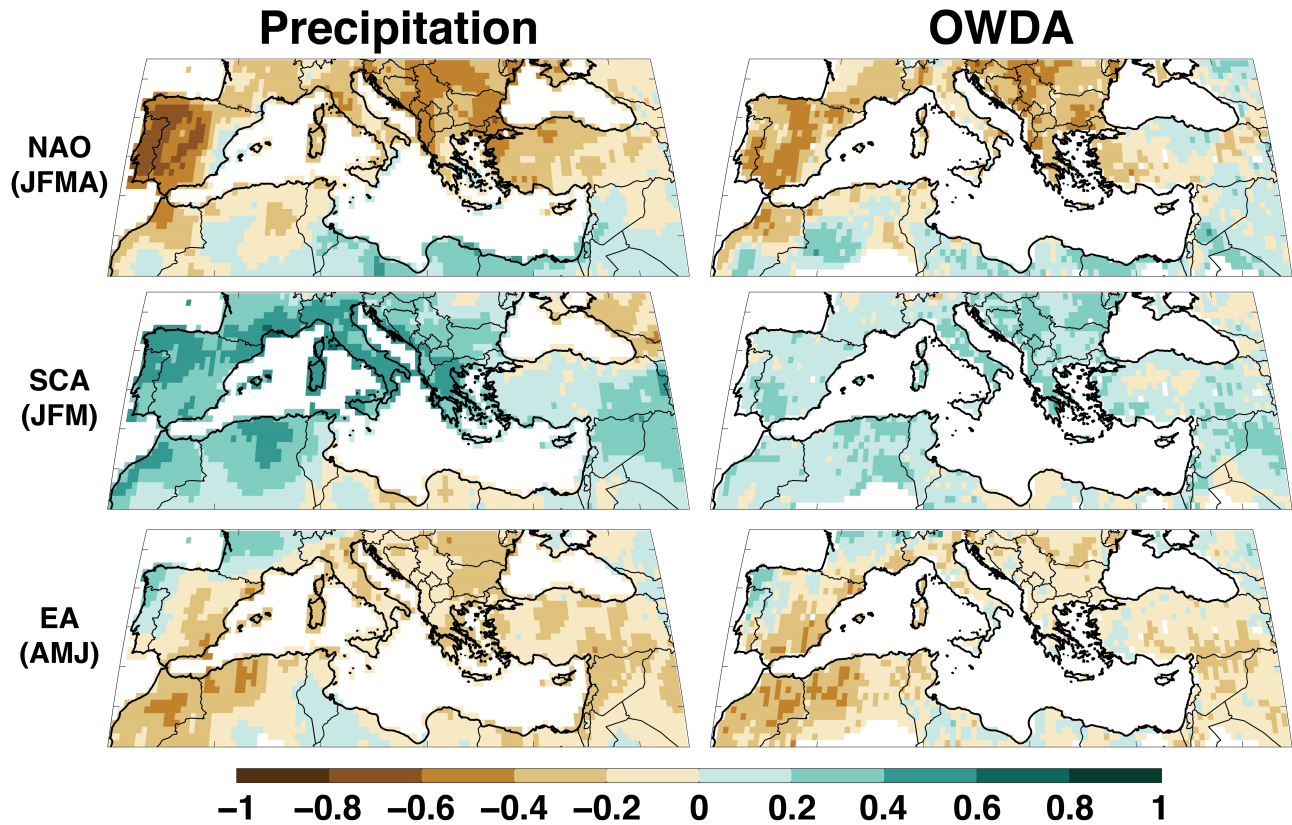


**Figure 3.** Spearman's rank correlation coefficients between the teleconnection indices (NAO, SCA, EA) and simultaneous season CRU 3.21 precipitation totals (left column) and OWDA summer season scPDSI (right column). Correlations are calculated over the period 1950–2012 CE.

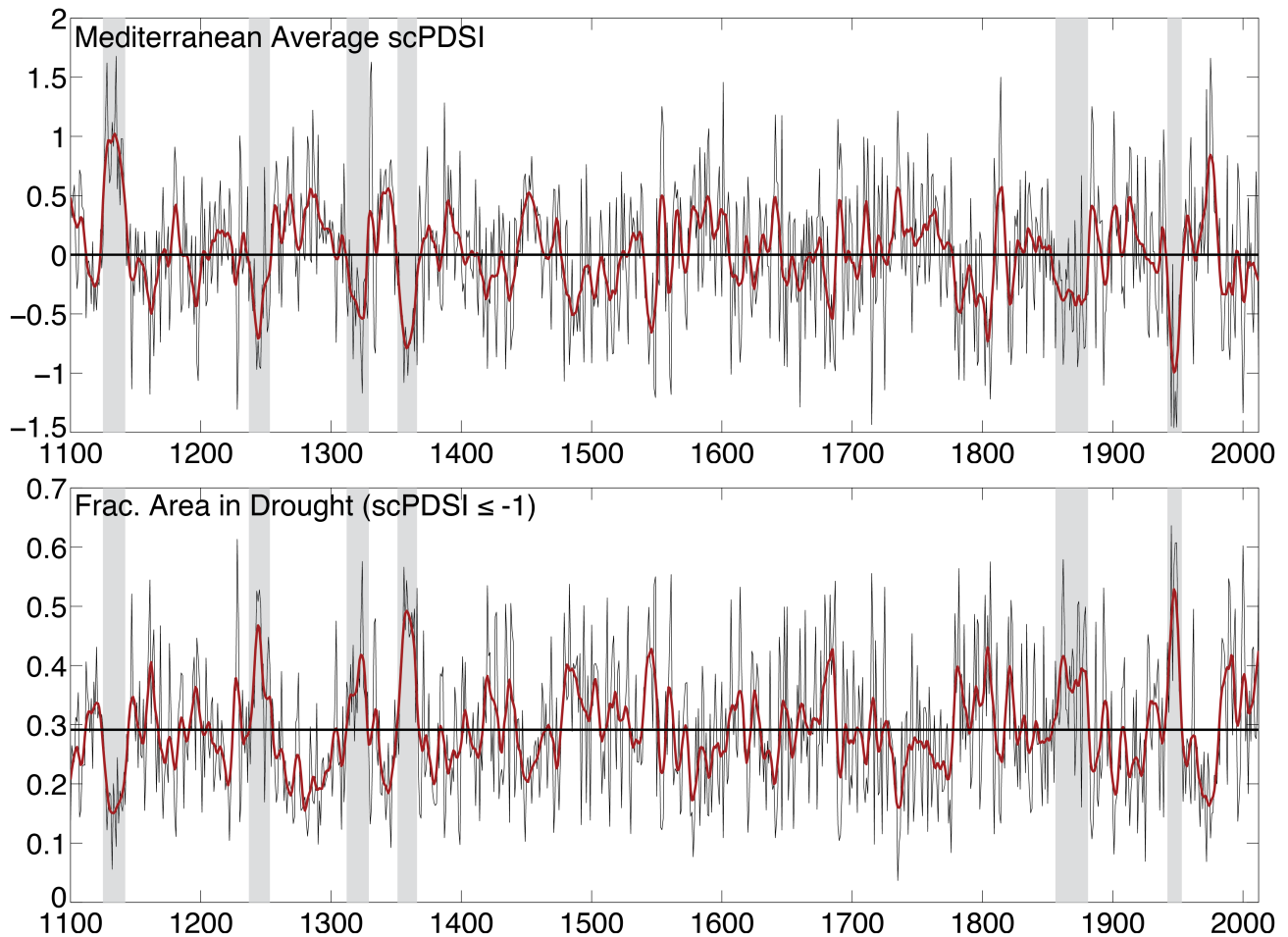


**Figure 4.** Area average scPDSI for the entire Mediterranean domain in the OWDA ( $30^{\circ}\text{N}$ – $47^{\circ}\text{N}$ ,  $10^{\circ}\text{W}$ – $45^{\circ}\text{E}$ ) (top) and percent land area in drought ( $\text{scPDSI} \leq -1$ ) (bottom) from 1100–2012 CE. Red curves are smoothed versions of the time series using a 10-year loess spline. The horizontal line in the lower panel is the long-term average fractional area in drought from 1100–2012 CE (29%). Highlighted in grey are several example periods of persistent pan-basin drought and pluvial events (see Figure 5).

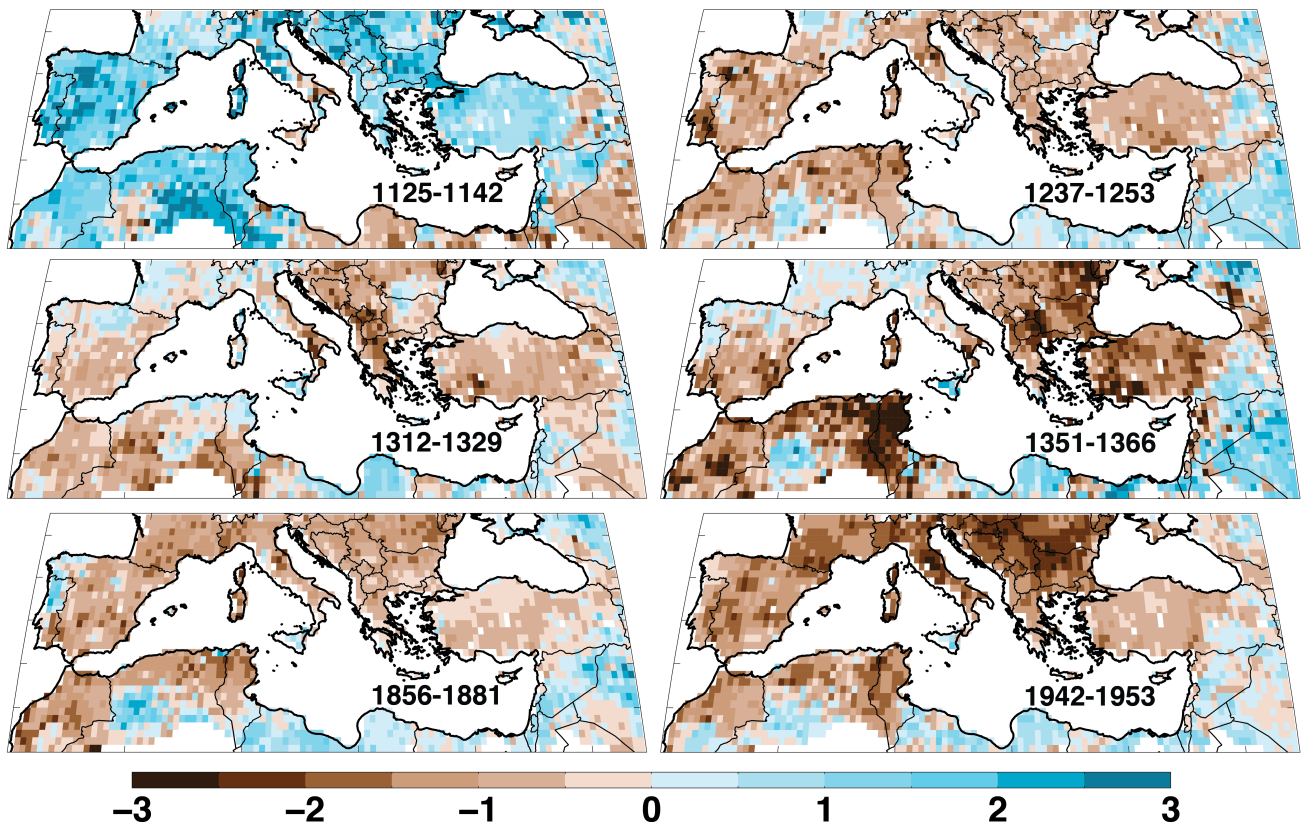


**Figure 5.** Multi-year average scPDSI for different pan-basin drought and pluvial events in the OWDA.

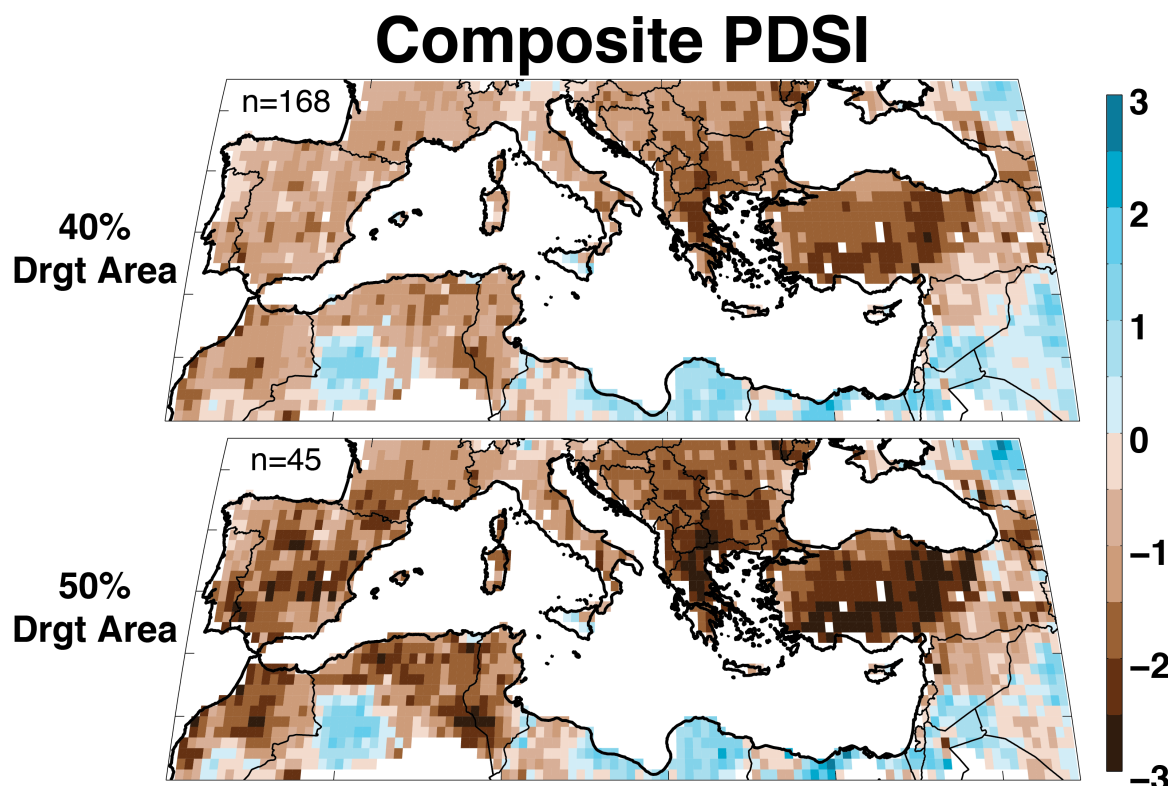


**Figure 6.** Composite average of Mediterranean drought events in the OWDA with a drought area ( $\text{scPDSI} \leq -1$ ) exceeding 40% ( $n = 168$  years) and 50% ( $n = 45$  years) of the total land area in the Mediterranean domain.

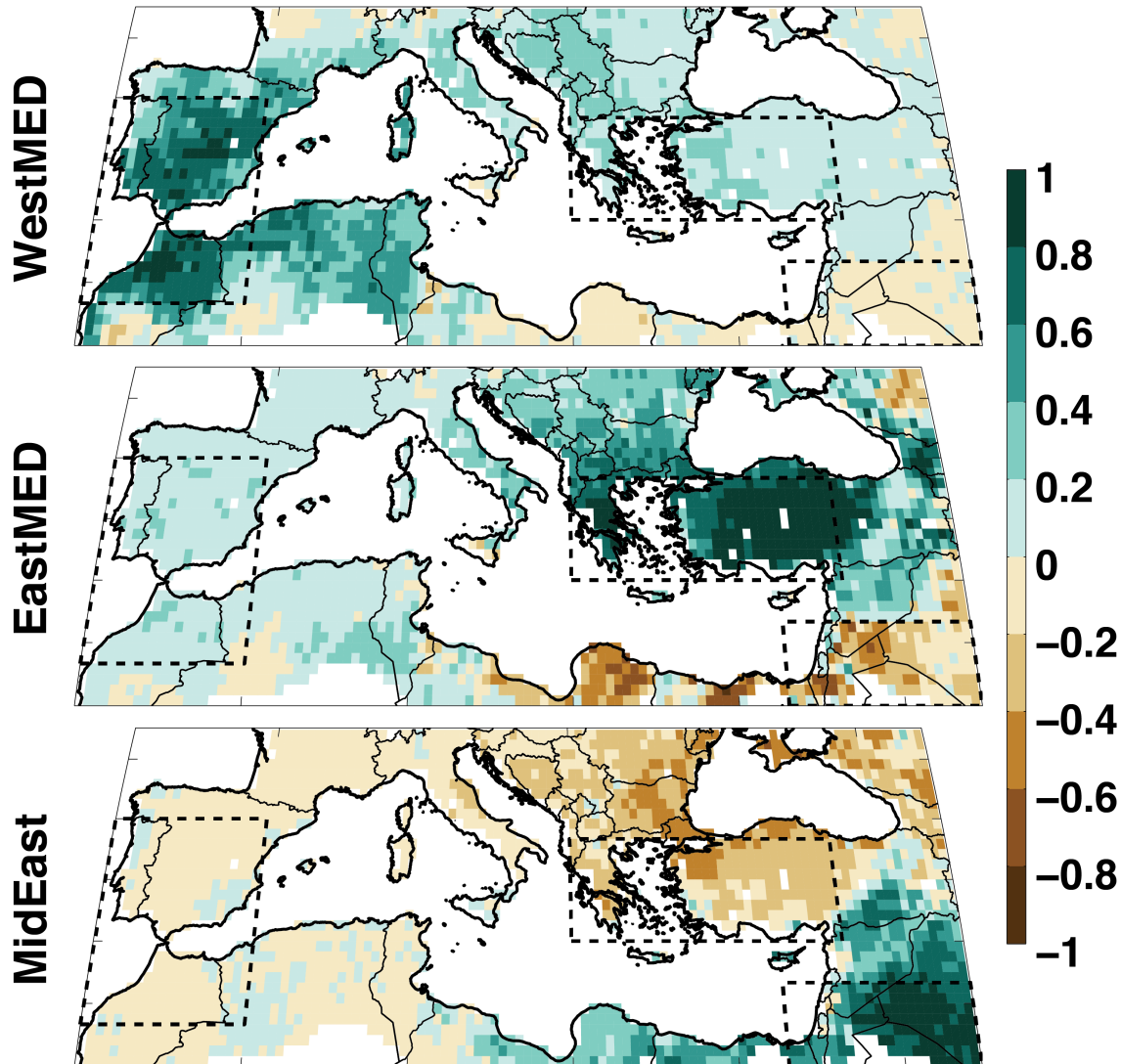


**Figure 7.** Point-by-point Spearman's rank correlations (1100–2012) between OWDA scPDSI and the Western Mediterranean (WestMED; 32°N–42°N, 10°W–0°), Eastern Mediterranean (EastMED; 36°N–41°N, 20°E–37°E), and Middle East (MidEast; 30°N–34°N, 33°E–47°E) regional average scPDSI time series.

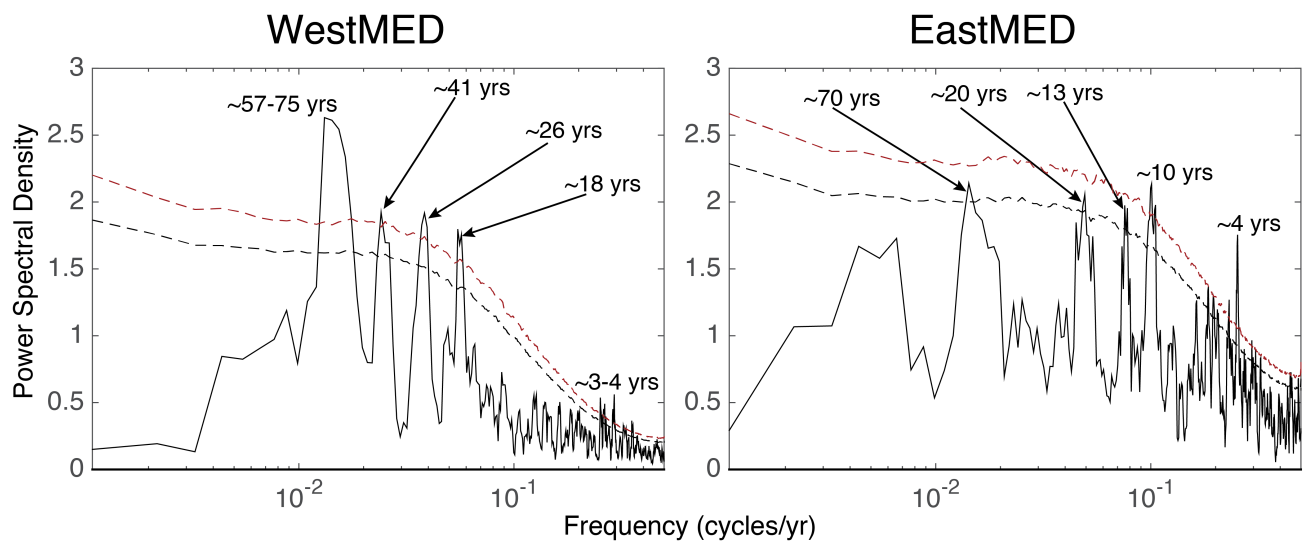


**Figure 8.** Power spectral density (Multi-taper Method, 3 tapers) for the WestMED and EastMED regional average scPDSI series. Red and black dashed lines are the 95<sup>th</sup> and 90<sup>th</sup> confidence limits, respectively, estimated from 10,000 AR(1) series generated from the original time series.

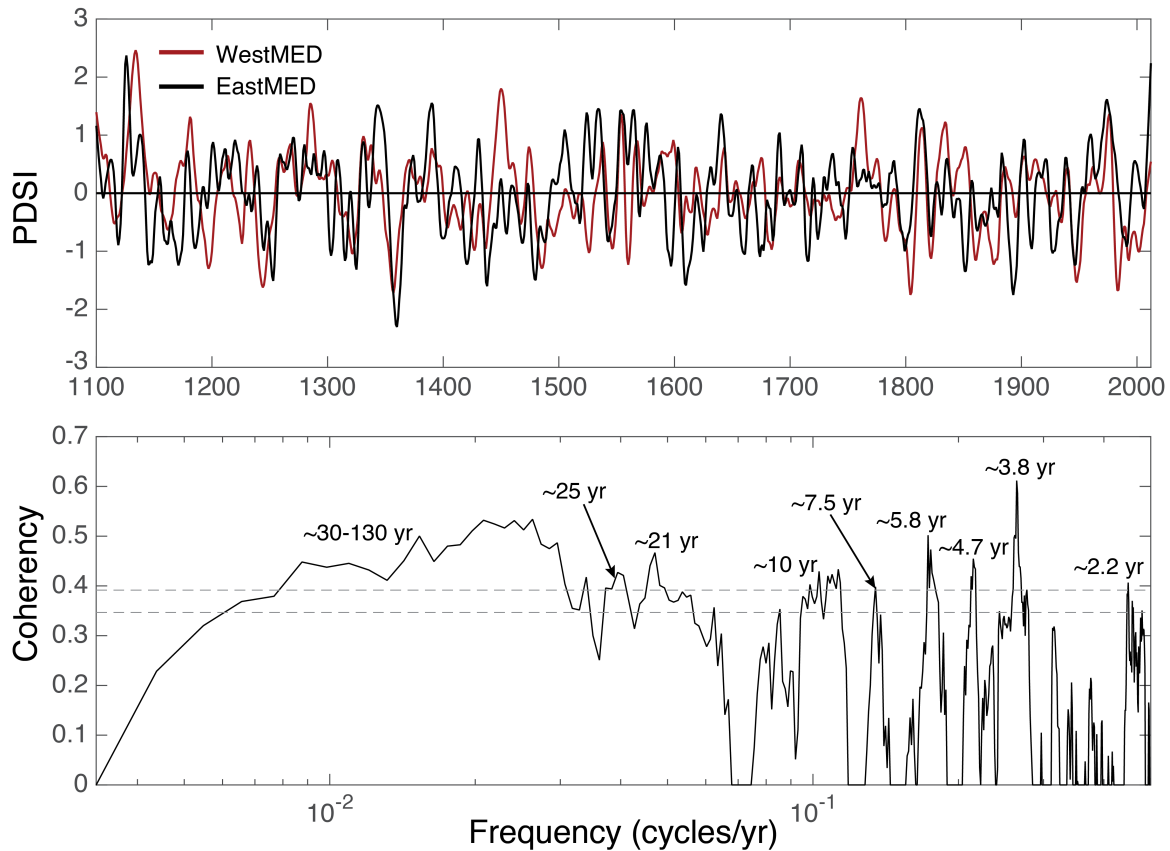


**Figure 9.** Smoothed versions (10-year loess spline) of the WestMED and EastMED time series (top) and the coherency spectra between the two unsmoothed series (bottom).

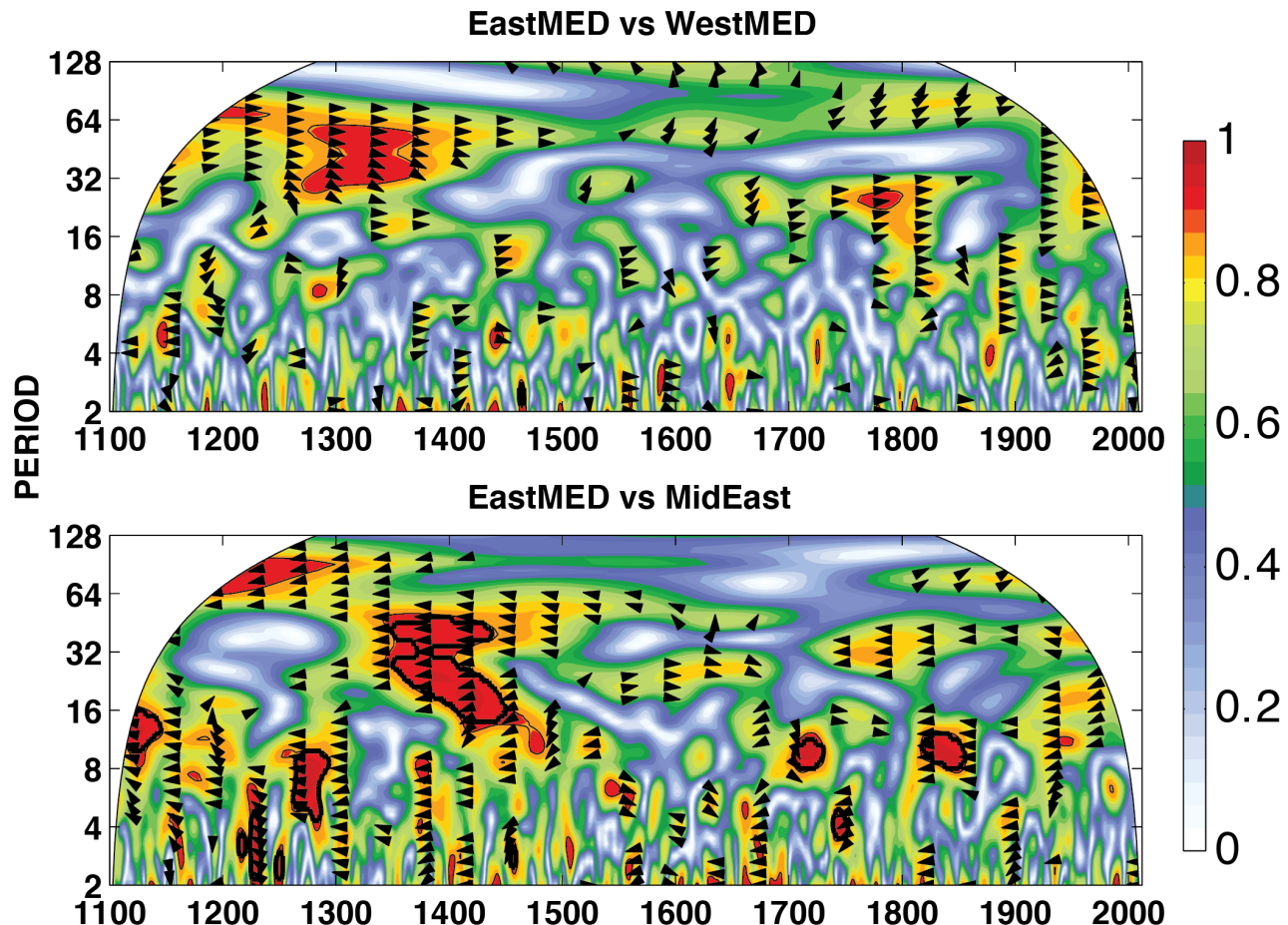


**Figure 10.** Squared wavelet coherence for EastMED versus WestMED (top) and EastMED versus MidEast (bottom). Black arrows pointing directly right indicate where the two time series have significant shared variance and are in phase; black arrows pointed left indicate where the two series are 180 degrees out of phase.

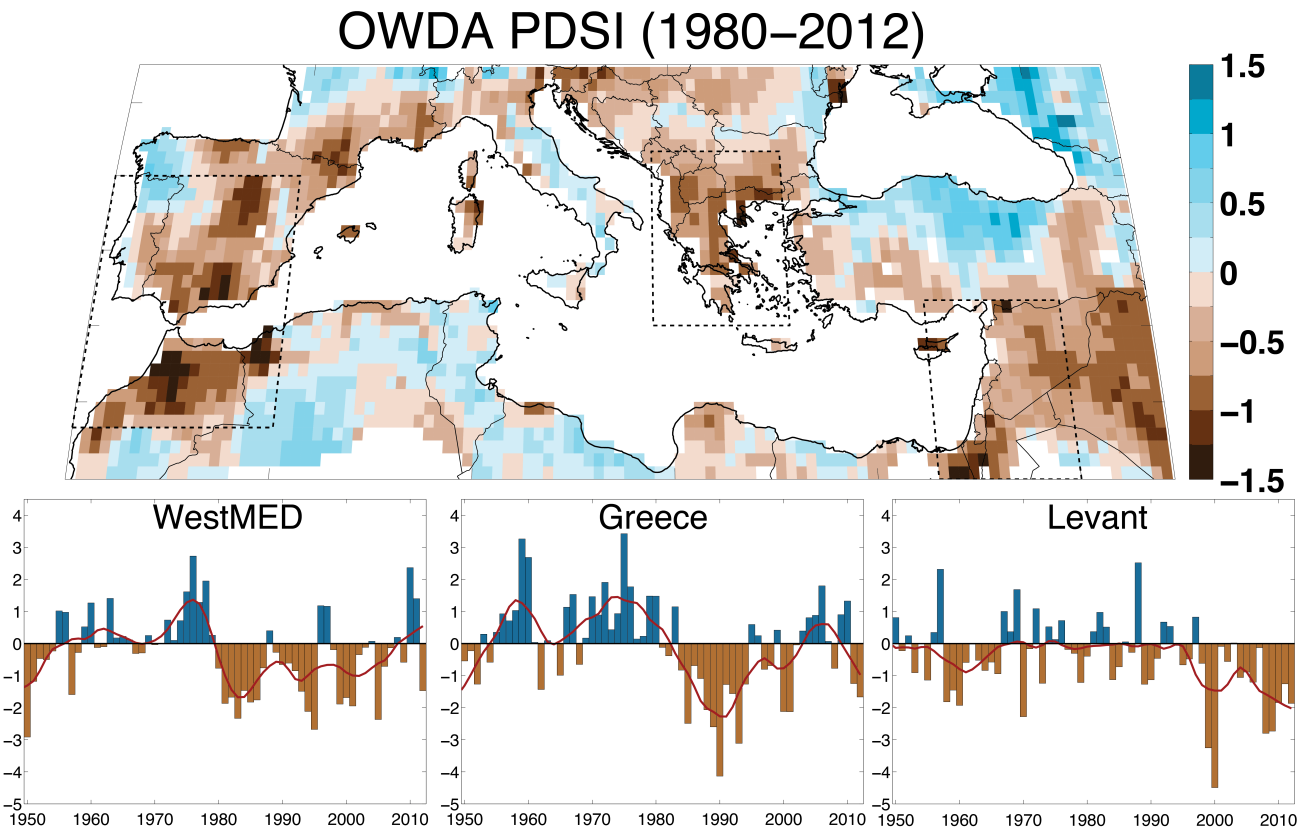


**Figure 11.** Multi-year average scPDSI for 1980–2012 (top) with regions of recent and persistent drought outlined in dashed black lines: WestMED ( $32^{\circ}\text{N}$ – $42^{\circ}\text{N}$ ,  $10^{\circ}\text{W}$ – $0^{\circ}$ ), Greece ( $36^{\circ}\text{N}$ – $43^{\circ}\text{N}$ ,  $19^{\circ}\text{E}$ – $26^{\circ}\text{E}$ ), and the Levant ( $30^{\circ}\text{N}$ – $37^{\circ}\text{N}$ ,  $33^{\circ}\text{E}$ – $40^{\circ}\text{E}$ ). Also shown (bottom) are the regional average scPDSI time series from these regions for 1950–2012 (red line is a 10-year loess smoother).

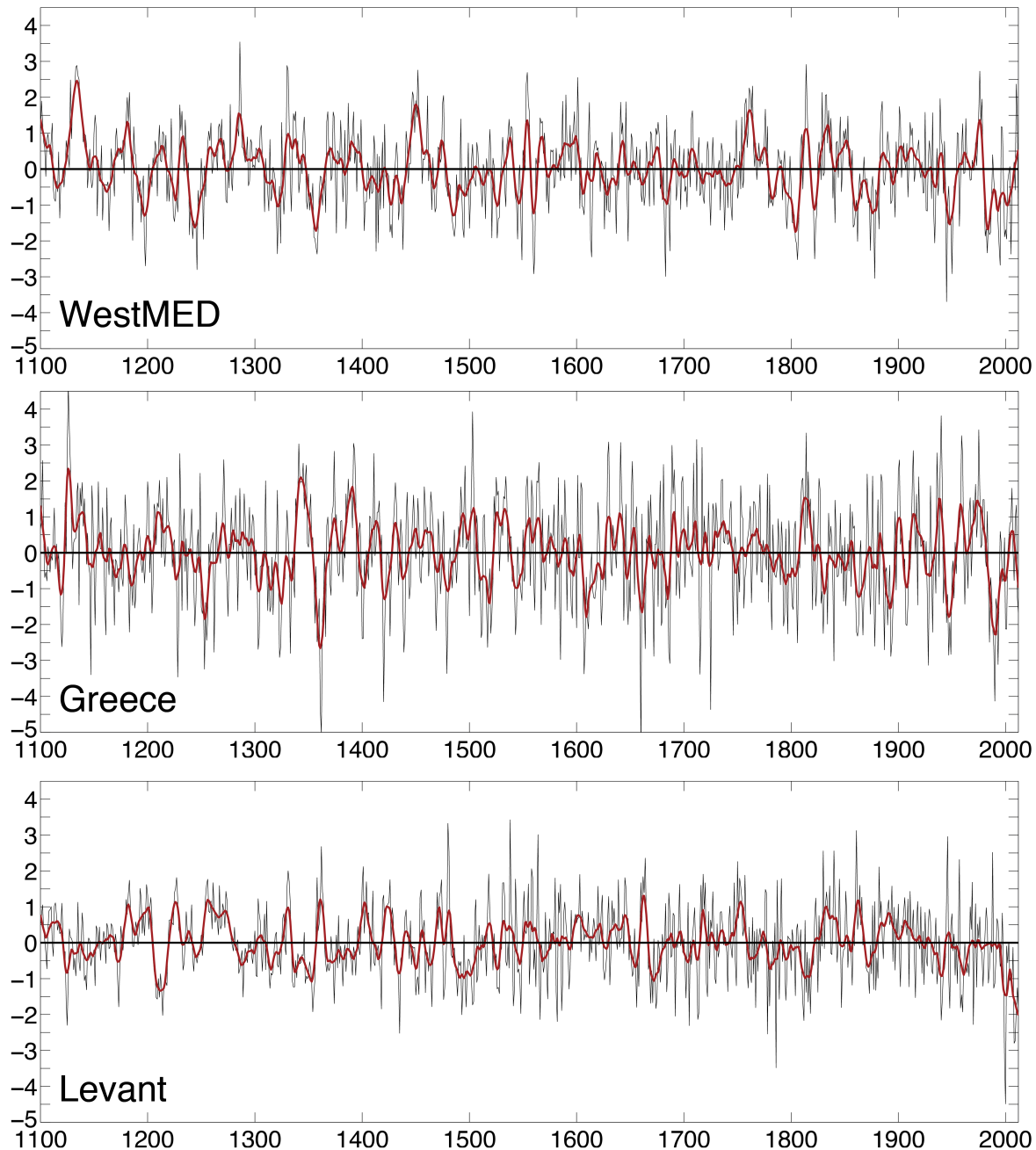


**Figure 12.** Re-centered (zero mean from 1100–2012 CE) time series for WestMED, Greece, and the Levant region. Red lines represent smoothed versions using a 10-year loess smoother.

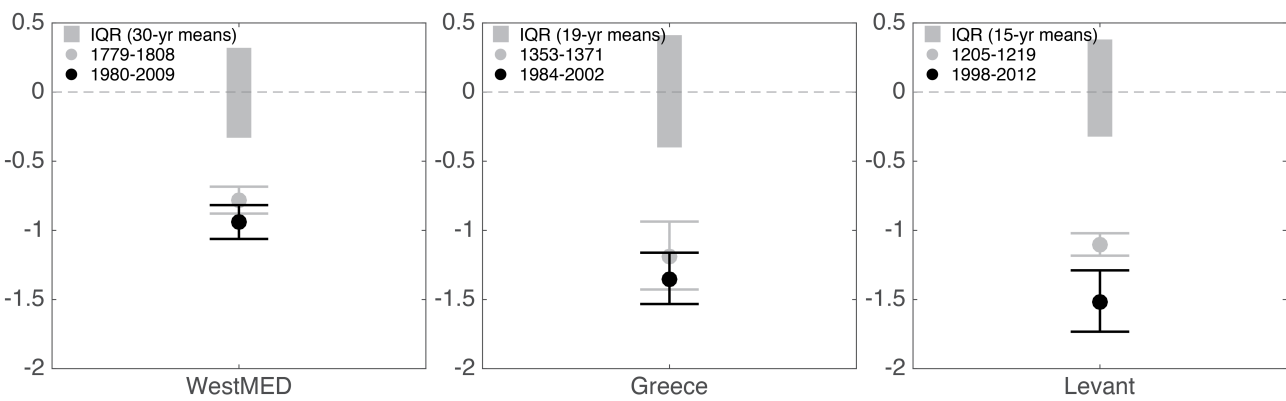


**Figure 13.** Comparisons between multi-year average re-centered scPDSI during recent decades (black dots) and driest previous periods of the same length in the OWDA from 1100–2012 CE. Grey bars are the interquartile range of mean PDSI for all such periods, grey dots represent the driest period prior to the recent decades, and black dots are the mean PDSI for the most recent drought. Whiskers are the 25<sup>th</sup> and 75<sup>th</sup> confidence limits for the dry events, estimated from 10,000 resamplings with replacement from scPDSI values during these intervals.